PNAS RESEARCH ARTICLE | NEUROSCIENCE

Tsc2 knockout counteracts ubiquitin-proteasome system insufficiency and delays photoreceptor loss in retinitis pigmentosa

Yixiao Wang[a], Claudio Punzo[b], John D. Ash[a], and Ekaterina S. Lobanova[a,c,1]

Edited by Gabriel Travis, David Geffen School of Medicine at UCLA, University of California, Los Angeles, CA; received October 19, 2021; accepted January 12, 2022 by Editorial Board Member Jeremy Nathans

Methods to stimulate protein degradation through the ubiquitin-proteasome system (UPS) are being investigated as approaches to treat multiple human diseases and delay aging. Recent studies highlighted a nontrivial relationship between the mammalian target of rapamycin complex 1 (mTORC1) pathway and the UPS. In different experimental models, both activation and inhibition of the mTORC1 pathway were reported to stimulate degradation of ubiquitinated proteins and proteasomal abundance. Here, we show that in rod photoreceptors, activation of mTORC1 through deletion of its negative regulator tuberous sclerosis complex protein 2 (Tsc2) counteracts UPS insufficiency, increases proteasomal activity, improves photoreceptor survival, and delays vision loss in a mouse model of human blindness caused by a misfolded protein. We show that an observed mTORC1-mediated increase in proteasomal activity was reduced by phosphatase treatment and could not be attributed to the change in proteasomal abundance. Our study indicates that chronic mTORC1 activation in vivo could stimulate the UPS in degenerating photoreceptor neurons. Further studies to understand changes in the degradation of ubiquitinated proteins and the modulation of UPS through phosphorylation under chronic mTORC1 activation might aid in the development of therapeutic approaches to diseases linked to impaired proteasomal degradation.

retinal degeneration | photoreceptor | proteasome | protein phosphorylation | mTORC1

Degenerative diseases of the retina are caused by a vast number of mutations in many individual genes (1–3). A potentially efficient strategy to treat these conditions would allow targeting pathways shared among multiple forms of degeneration. Previously, we and others reported that rod photoreceptors of several mouse models of retinal degeneration accumulate the ubiquitin-proteasome reporter, Ub^{G76V}-GFP, indicating impaired processing of ubiquitinated proteins (4–7). Reporter accumulation was observed in rods expressing misfolded proteins (mutant P23H rhodopsin and transducin beta subunit) and rods experiencing problems with building outer segments (peripherin and rhodopsin knockout mice) (4, 5). Other groups reported accumulation of the reporter in BBS5 and Lrat knockout mice (6, 7). Whether the rate-limiting steps for processing ubiquitinated proteins in these diverse mouse models are the same is currently unknown. It is also unknown which specific changes in degenerating rods interfere with and delay the processing of the Ub^{G76V}-GFP reporter, leading to its accumulation. Nonetheless, all of these studies point to UPS (ubiquitin-proteasome system) insufficiency as a potential stress factor contributing to photoreceptor degeneration in many forms of retinal degeneration. Therefore, approaches to stimulate processing of ubiquitinated proteins and relieve UPS insufficiency may be an effective way to treat a broad spectrum of retinal degenerations.

A number of recent studies bring attention to the complex relationship between the mTORC1 (mammalian target of rapamycin complex 1) and degradation of ubiquitinated proteins: in diverse experimental systems, the UPS is regulated by mTORC1, both positively and negatively (8–15). One of the debated questions is the consequence of mTORC1 inhibition or activation on proteasome abundance and activity. Both inhibition and activation of mTORC1 were reported to increase proteasomal expression (11, 15). Chronic genetic activation of mTORC1 was reported to stimulate degradation of ubiquitinated proteins in mouse fibroblasts, potentially through an increase in the transcriptional biogenesis of proteasomal subunits (15). Furthermore, embryonic retinas of mice with activated mTORC1 were reported to have higher levels of proteasomes (16). Building on these two findings, we explored activation of mTORC1 as an approach to generate more proteasomes and stimulate degradation of ubiquitinated proteins in degenerating photoreceptors with UPS insufficiency.

Significance

Studies in multiple experimental systems have demonstrated that an increase in proteolytic capacity of post-mitotic cells improves cellular resistance to a variety of stressors, delays cellular aging and senescence. Therefore, approaches to increase the ability of cells to degrade misfolded proteins could potentially be applied to the treatment of a broad spectrum of human disorders. An example would be retinal degenerations, which cause irreversible loss of vision and are linked to impaired protein degradation. This study suggests that chronic activation of the mammalian target of rapamycin complex 1 (mTORC1) pathway in degenerating photoreceptor neurons could stimulate the degradation of ubiquitinated proteins and enhance proteasomal activity through phosphorylation.

Author contributions: Y.W. and E.S.L. designed research; Y.W. performed research; C.P. contributed new reagents/analytic tools; Y.W., J.D.A., and E.S.L. analyzed data; E.S.L. wrote the paper; and J.D.A. edited the manuscript.

The authors declare no competing interest.

This article is a PNAS Direct Submission. G.T. is a guest editor invited by the Editorial Board.

[1]To whom correspondence may be addressed. Email: elobanova@ufl.edu.

This article contains supporting information online at http://www.pnas.org/lookup/suppl/doi:10.1073/pnas.2118479119/-/DCSupplemental.

Published March 11, 2022.

We report that genetic activation of mTORC1 improved clearance of the UPS reporter, stimulated proteasomal activity, and delayed visual loss in a preclinical model of human blindness caused by a misfolded P23H rhodopsin mutant. Surprisingly, we found that mTORC1-mediated increase in proteasomal activity was almost entirely phosphorylation-dependent and could not be attributed to higher proteasomal levels. Further studies of poorly understood mTORC1/UPS connections and changes in UPS regulation under chronic activation of mTORC1 pathway might bring new ideas for the development of tools to manipulate degradation of ubiquitinated proteins.

Results

The stimulation of the mTORC1 pathway can be achieved by deleting one of its negative regulators, the tuberous sclerosis complex protein 2 (Tsc2). We accomplished this specifically in rod photoreceptors by crossing mice bearing a Tsc2-floxed allele ($Tsc2^{fl/fl}$) and mice expressing Cre recombinase in rods (17, 18). The effects of genetic activation of mTORC1 on proteostasis were studied in heterozygote $Rho^{P23H/WT}$ knock-in mice, an established model of retinitis pigmentosa. In these mice, a P23H substitution in rhodopsin leads to its misfolding, which requires its constant degradation stressing rod photoreceptors to their eventual demise (19, 20). Previous studies of rod-specific Tsc1 and Tsc2 knockout mice showed slow age-related development of RPE (retinal pigment epithelium) and vascular pathology, increased signs of inflammation without dramatic loss of photoreceptors at least until 1 y of age (21, 22). The slow-developing and minor photoreceptor pathology caused by the Tsc2 knockout is not expected to overcomplicate our studies of $Rho^{P23H/WT}$ mice, which lose the majority of their rod photoreceptors by 6 mo (19, 20). Mice lacking the Tsc2 gene in rods ($Rho^{P23H/WT}/Tsc2^{Rod\,KO}$) were compared with $Rho^{P23H/WT}$ littermates, and rod-specific Tsc2 knockout mice (abbreviated as $Tsc2^{Rod\,KO}$) were compared with their wild type littermates (abbreviated as WT and $Tsc2^{fl/fl}$).

In the initial set of experiments, we confirmed that rod-specific Tsc2 knockout stimulates the mTORC1 pathway by conducting Western blot analysis of retinal extracts (Fig. 1). Activation of mTORC1 was evident from increased phosphorylation of mTOR and major downstream phosphorylation targets of mTORC1, such as 4E-BP1 (eukaryotic translation initiation factor 4E-binding protein 1) and S6K1 (ribosomal protein S6 kinase beta-1). Similar changes in protein markers of the mTORC1 pathway were observed in $Tsc2^{Rod\,KO}$ mice compared to WT littermate mice.

Rod-Specific Tsc2 Knockout Improves Photoreceptor Survival and Delays Vision Loss in P23H Mice. First, to establish that rod-specific Tsc2 knockout delays retinal degeneration in $Rho^{P23H/WT}$ mice, we used noninvasive in vivo imaging methods, optical coherence tomography (OCT) and fundoscopy. By 6 mo of age, the fundus images of $Rho^{P23H/WT}$ mice had large pigmented areas, indicating a dramatic thinning of the retina (Fig. 2 *C*, *Upper*). Consistently, the thickness of the outer nuclear layer (ONL) in OCT scans, which correlates with the number of rod photoreceptors, was hardly discernable in degenerating 6-mo-old $Rho^{P23H/WT}$ mice (Fig. 2 *C*, *Bottom*; marked in red). In contrast, the ONL in the retinas of age-matched $Rho^{P23H/WT}/Tsc2^{Rod\,KO}$ mice was clearly thicker (Fig. 2 *C*, *Lower*). A formal analysis of the ONL thickness around the optic nerve head (ONH) presented in the form of OCT spider diagrams showed approximately threefold better preservation of

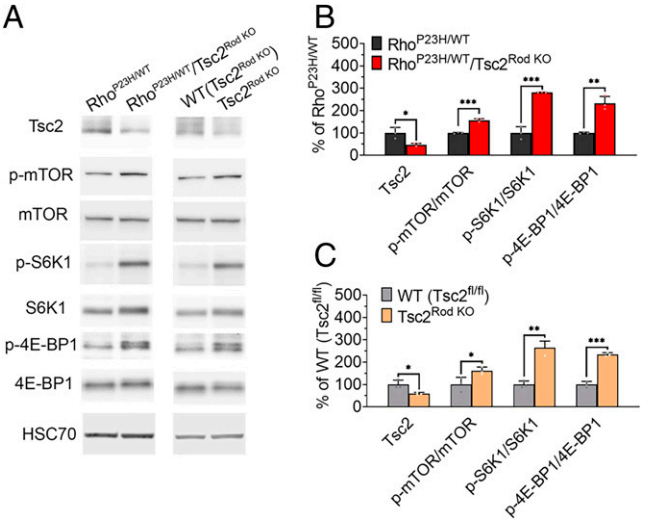

Fig. 1. Rod-specific Tsc2 knockout stimulates mTORC1 pathway. (*A*) Representative Western blots and (*B* and *C*) density plots for Tsc2, mTOR, and its phosphorylated form (p-mTOR), and major phosphorylation targets of mTORC1 (4E-BP1, S6K1) detected in the retinal extracts prepared from mice of the indicated genotypes. Values are shown as a percentage of average values for $Rho^{P23H/WT}$ or WT ($Tsc2^{fl/fl}$) littermate mice. Representative results from at least four independent experiments for each mouse line are shown. All animals are 1 mo old. Uncropped images of Western blots are shown in *SI Appendix*, Fig. S1. $*P < 0.05$, $**P < 0.01$, $***P < 0.001$, and ns for $P > 0.05$.

photoreceptors (Fig. 2*F*). Spider diagrams showed ∼20% more surviving photoreceptors in mice as young as 6 to 7 wk (Fig. 2 *A* and *D*) and approximately twofold preservation of photoreceptors in 3-mo-old $Rho^{P23H/WT}/Tsc2^{Rod\,KO}$ mice (Fig. 2 *B* and *E*). Overall, the fundoscopic images and OCT spider diagrams of 6-mo-old $Rho^{P23H/WT}/Tsc2^{Rod\,KO}$ mice resemble the images and diagrams from younger 3-mo-old $Rho^{P23H/WT}$ mice, suggesting a delay in photoreceptor loss by ∼3 mo (see also *SI Appendix*, Fig. S2).

A similar imaging analysis did not show differences between young $Tsc2^{Rod\,KO}$ and WT littermates (Fig. 2 *G* and *H*). Approximately 25% of Cre-positive Tsc2 mice over 4 mo of age had occasional ∼50- to 80-μm bright spots on the funduscopic images, which continued to grow with age (Fig. 2*I*). OCT scans indicated that these spots corresponded to localized distortions of the outer limiting membranes (OLMs) and have an appearance of retinal in-folds (Fig. 2*I*; see also Movie S1). These observations are similar to the age-related development of retinal in-folds previously described in rod-Tsc1 and Tsc2 knockouts (21, 22). Formation of retinal in-folds in $Rho^{P23H/WT}/Tsc2^{Rod\,KO}$ mice was never observed.

Next, we confirmed improved photoreceptor survival in $Rho^{P23H/WT}/Tsc2^{Rod\,KO}$ mice with morphometric analysis (Fig. 3). We analyzed retinal cross-sections cut through the optic nerve along the superior-inferior line. The results were plotted as spider diagrams representing counts of photoreceptor nuclei in 100-μm segments at different distances from the ONH (Fig. 3 *A* and *B*, *Middle*). These data demonstrate an improvement in photoreceptor preservation throughout the entire retina (Fig. 3 *A* and *B*, *Middle*; see also *SI Appendix*, Fig. S3). At 3 mo of age, $Rho^{P23H/WT}/Tsc2^{Rod\,KO}$ mice retained twice as many photoreceptors compared to their $Rho^{P23H/WT}$ littermates (Fig. 3 *A*, *Right*). By the age of 6 mo, the ONL in $Rho^{P23H/WT}$ retinas were reduced to only one or two rows of the nuclei in the superior part near the optic nerve (Fig. 3 *B*, *Left*). In contrast, $Rho^{P23H/WT}/Tsc2^{Rod\,KO}$ mice had approximately four to six rows of photoreceptor nuclei, indicating approximately threefold

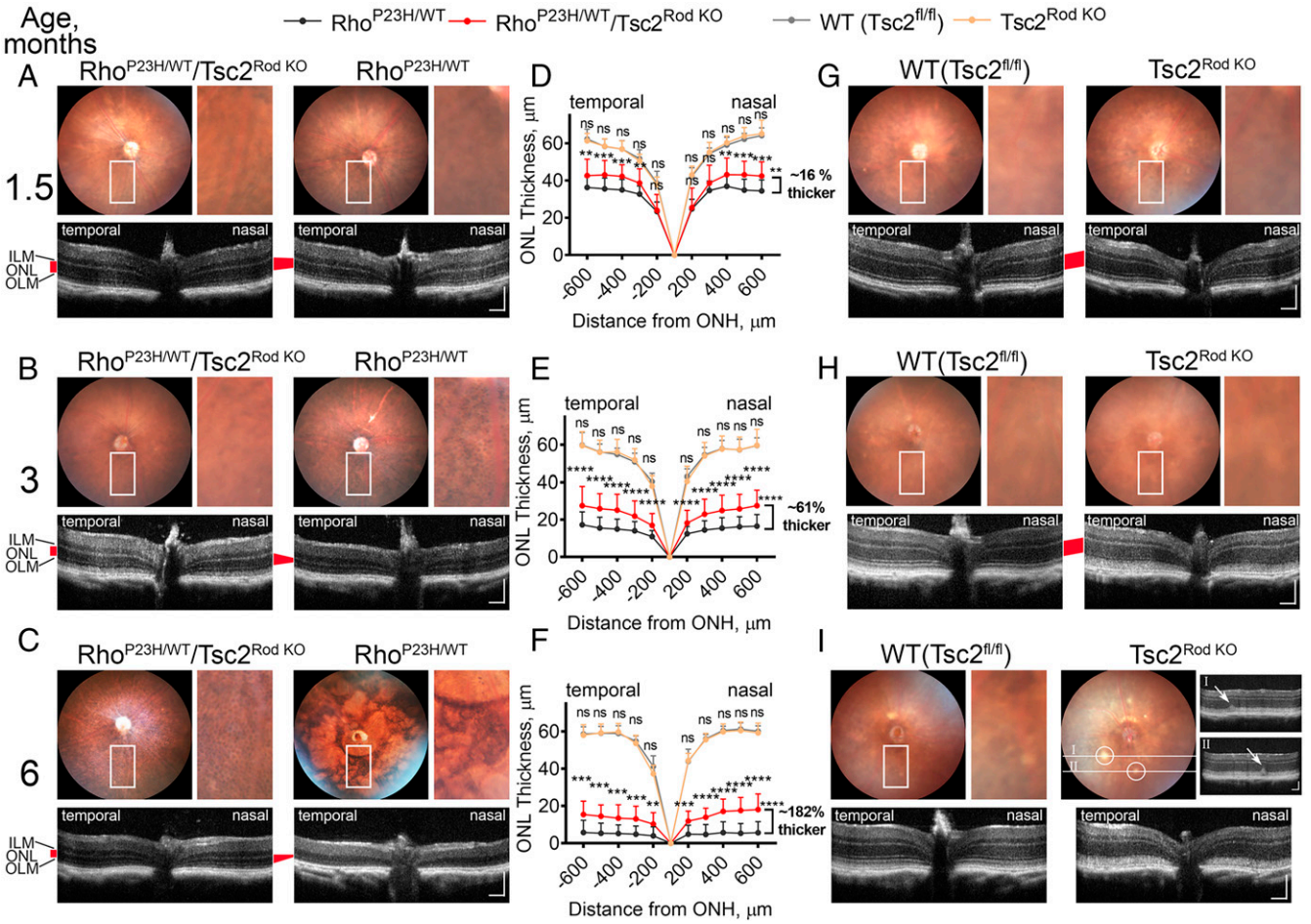

Fig. 2. Rod-specific Tsc2 knockout supports retinal preservation in a $Rho^{P23H/WT}$ mouse model of retinitis pigmentosa. (*A–C*, *G*, and *H*); representative funduscopic images (*Top*) and horizontal SD-OCT scans (*Bottom*). (*D–F*) Horizontal OCT spider diagrams of ONL thickness for mice of indicated genotypes at 1.5 (*A*, *D*, and *G*), 3 (*B*, *E*, and *H*), and 6 (*C*, *F*, and *I*) months of age. ILM: inner limiting membrane, ONL: outer nuclear layer, OLM: outer limiting membrane. (OCT images scale bar, 100 μm.) The ONL on OCT images is marked with a red quadrilateral. To estimate ONL thickness changes, the measurements from an OCT spider diagram for each $Rho^{P23H/WT}/Tsc2^{Rod\ KO}$ mouse were summed, averaged, and expressed as a percentage of average values for $Rho^{P23H/WT}$ mice. The numbers of eyes analyzed at 1.5 mo were as follows: $Rho^{P23H/WT}$ – 21, $Rho^{P23H/WT}/Tsc2^{Rod\ KO}$ – 27, WT – 9, $Tsc2^{Rod\ KO}$ – 7; at 3 mo: $Rho^{P23H/WT}$ – 40, $Rho^{P23H/WT}/Tsc2^{Rod\ KO}$ – 26, WT – 14, $Tsc2^{Rod\ KO}$ – 14; and at 6 mo: $Rho^{P23H/WT}$ – 16, $Rho^{P23H/WT}/Tsc2^{Rod\ KO}$ – 14, WT – 14, $Tsc2^{Rod\ KO}$ – 17. The OCT scans are assembled as Movie S1. $^{**}P < 0.01$, $^{***}P < 0.001$, $^{****}P < 0.0001$, and ns for $P > 0.05$.

preservation of photoreceptors. The numbers of nuclei in the photoreceptor layer in $Tsc2^{Rod\ KO}$ and wild-type littermates ($Tsc2^{fl/fl}$) were indistinguishable (Fig. 3 *A* and *B*, *Middle*; see also *SI Appendix*, Fig. S4). This is consistent with aforementioned reports that rod-specific Tsc1 and Tsc2 knockout mice lose photoreceptors very slowly with age (21, 22).

Finally, using electroretinography (ERG), we confirmed that better photoreceptor preservation in $Rho^{P23H/WT}/Tsc2^{Rod\ KO}$ retinas translates into improved retinal function (Fig. 4). Dark-adapted mice were exposed to bright flashes of increasing intensity using protocols allowing assessment of scotopic (rods), mesopic (mixed rods and cones), and photopic vision (cones) (23). The a-wave of the ERG response originates primarily from rod and cone photoreceptors. The b-wave represents amplified responses by downstream retinal neurons. In degenerating retinas, any changes in the amount and health of surviving photoreceptors are reflected by reduced amplitudes of both waves. At 3 and 6 mo of age (Fig. 4 *A* and *B*), visual responses of $Rho^{P23H/WT}/Tsc2^{Rod}$ mice yielded higher a- and b-wave amplitudes in comparison to $Rho^{P23H/WT}$ mice. ERG responses recorded from $Tsc2^{Rod\ KO}$ and their wild-type littermate mice ($Tsc2^{fl/fl}$) using the same protocol were indistinguishable from one another.

The Knockout of Tsc2 Counteracts UPS Insufficiency in Degenerating Rods of $Rho^{P23H/WT}$ Mice. In the following experiments, we evaluated changes in the major proteostasis branches, including UPS, autophagy, and protein translation. First, we showed that genetic activation of mTORC1 affects the UPS insufficiency in $Rho^{P23H/WT}$ rods. We took advantage of the transgenic mouse expressing the Ub^{G76V}-GFP proteasomal sensor (24–26). As we have previously shown, in healthy photoreceptors, the Ub^{G76V}-GFP proteasomal sensor is quickly targeted to proteasomes for degradation and is barely detectable (4). However, it accumulates in rods of $Rho^{P23H/WT}$ mice, reflecting the insufficiency of their UPS functioning (5). As shown in Fig. 5*A*, using confocal immunofluorescence microscopy, we observed a significant reduction of the reporter level in rods of $Rho^{P23H/WT}/Tsc2^{Rod\ KO}$ mice in comparison to $Rho^{P23H/WT}$ littermates. We next used Western blot analysis to confirm and estimate an approximately fourfold reduction of reporter signal (Fig. 5*B*, lanes 4 and 5; Fig. 5*D*). In $Tsc2^{Rod\ KO}$ control mice, the Ub^{G76V}-GFP sensor was barely detectable, and its level was similar to that in the retinas of healthy WT littermates (Fig. 5 *C* and *D*).

The ability of the mTORC1 pathway to affect cellular proteostasis through modulation of autophagy and protein

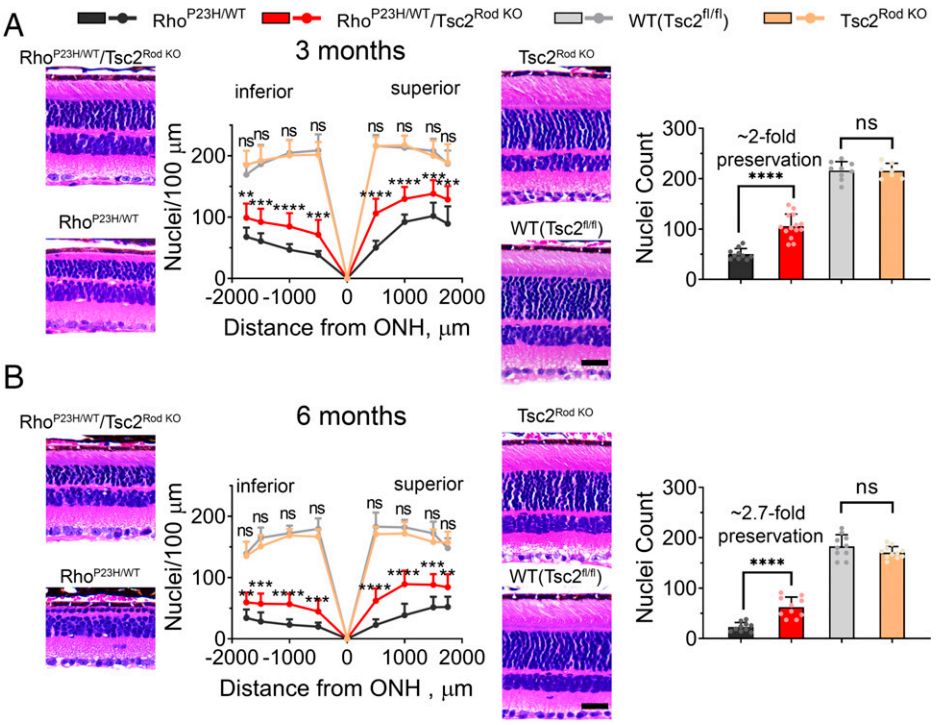

Fig. 3. Rod-Tsc2 knockout delays photoreceptor loss in Rho$^{P23H/WT}$ mice. Morphometric analysis of retinas from (*A*) 3- and (*B*) 6-mo-old mice of indicated genotypes. Spider diagrams represent the number of photoreceptor nuclei in 100-μm segments counted along the inferior-superior axis of the mouse eye at various distances from the center of the ONH. Representative images of H&E-stained retinal cross-sections are taken in the superior part of the retina at ~500 μm distance from the center of the ONH. (Scale bars, 25 μm.) The representative cross-sections through an entire retina are shown in *SI Appendix*, Figs. S3 and S4. (*Right*) Nuclei count in 100-μm retinal segments in the superior part of the retina at 500 μm distance from the ONH. The numbers of eyes analyzed at 3 mo were as follows: Rho$^{P23H/WT}$ – 10, Rho$^{P23H/WT}$/Tsc2$^{Rod\ KO}$ – 14, WT – 9, Tsc2$^{Rod\ KO}$ – 7.The numbers of eyes analyzed at 6 mo were as follows: Rho$^{P23H/WT}$ – 10, Rho$^{P23H/WT}$/Tsc2$^{Rod\ KO}$ – 10, WT – 10, Tsc2$^{Rod\ KO}$ – 11. $^{**}P < 0.01$, $^{***}P < 0.001$, $^{****}P < 0.0001$, and ns for $P > 0.05$.

translation is well established in multiple experimental systems (27–29). Therefore, in the next set of experiments, we investigated whether better clearance of the UPS reporter in Rho$^{P23H/WT}$/Tsc2$^{Rod\ KO}$ mice could be attributed to higher autophagic activity or a reduced protein translation rate.

The autophagy-lysosomal pathway is the second proteolytic system responsible for the bulk engulfment and degradation of cytoplasmic material, organelles, large protein complexes, and protein aggregates. We noted slightly elevated levels of LC3-I and LC3-II (MAP1LC3-I/II [microtubule-associated protein 1

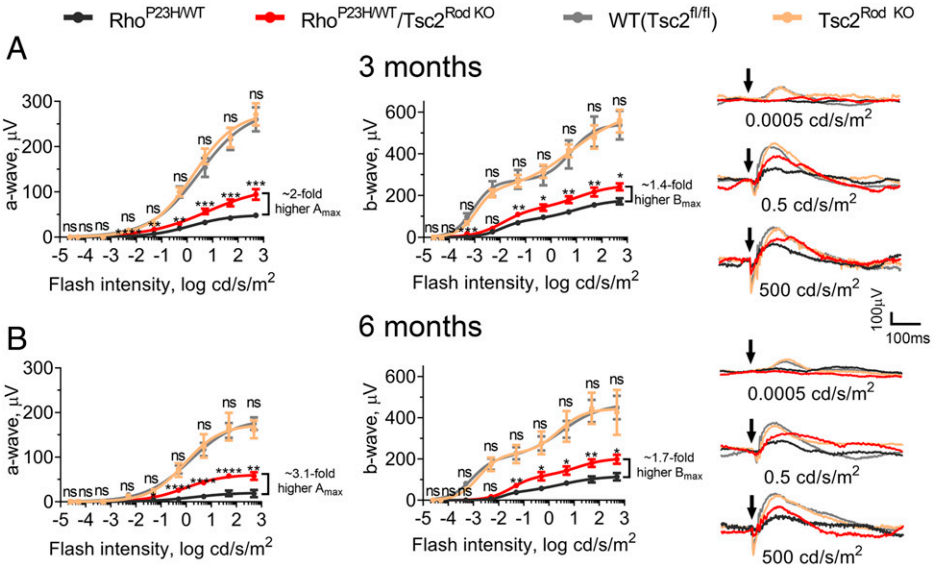

Fig. 4. Rod-specific Tsc2 knockout delays vision loss in Rho$^{P23H/WT}$ mice. Response amplitudes of ERG a- and b-waves evoked by light flashes of increasing intensity from mice of indicated genotypes were collected at 3 (*A*) and 6 (*B*) months of age. The numbers of eyes analyzed at 3 mo were as follows: Rho$^{P23H/WT}$ – 14, Rho$^{P23H/WT}$/Tsc2$^{Rod\ KO}$ – 10, WT (Tsc2$^{fl/fl}$) – 14, Tsc2$^{Rod\ KO}$ – 14. The numbers of eyes analyzed at 6 mo were as follows: Rho$^{P23H/WT}$ – 12, Rho$^{P23H/WT}$/Tsc2$^{Rod\ KO}$ – 10, WT (Tsc2$^{fl/fl}$) – 16, Tsc2$^{Rod\ KO}$ – 8. (*Right*) Representative ERG recordings evoked by flashes of indicated intensities representing scotopic, mesopic, and photopic light intensity ranges. A_{max} and B_{max} stand for maximum values of a- and b-waves recorded at saturating levels of light. Data are presented as mean ± SEM. $^{*}P < 0.05$, $^{**}P < 0.01$, $^{***}P < 0.001$, $^{****}P < 0.0001$, and ns for $P > 0.05$.

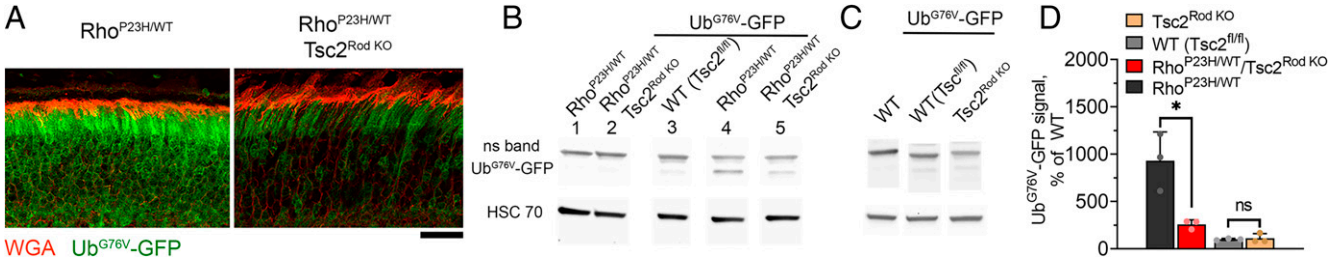

Fig. 5. Rod-specific Tsc2 knockout counteracts proteasomal insufficiency in Rho$^{P23H/WT}$ mice. (*A*) Ub^{G76V}-GFP reporter fluorescence (green) in retinal cross-sections of Rho$^{P23H/WT}$ and Rho$^{P23H/WT}$/Tsc2$^{Rod\ KO}$ littermate mice. Rod outer segments are stained with WGA conjugated to Alexa Fluor 555 (red). (Scale bar, 25 μm.) (*B* and *C*) Western blot detection of the Ub^{G76V}-GFP sensor in whole retina lysates from mice of indicated genotypes with the anti-GFP antibodies. Extracts obtained from littermates negative for the Ub^{G76V}-GFP transgene were used to control for antibody specificity. A nonspecific band detected with anti-GFP antibody is marked as "ns band." (*D*) The quantification plot for Western blot bands of the reporter is shown as a percentage of the average signal in WT/Ub^{G76V}-GFP mice. All animals are 1 mo old. Uncropped images of Western blots are shown in *SI Appendix*, Fig. S1. *$P < 0.05$, and ns for $P > 0.05$.

light chain 3 I/II]) autophagy markers in rod-Tsc2 retinas without changes in their ratio (Fig. 6). The levels of the other autophagy marker, SQSTM1 (sequestosome-1), did not change.

It is understood that levels of LC3-I and LC3-II represent a static picture, and alterations in their levels could be observed in the absence of changes in autophagy (30). Therefore, following standards in the field, to investigate changes in autophagic degradation activity, we measured autophagic flux, an accumulation of the phagosomal membrane marker LC3-II in the presence of autophagy inhibitors (30, 31).

Animals of each genotype were given an intraperitoneal injection of high doses of chloroquine (CQ) to inhibit autophagy, and accumulation of LC3-II was studied by Western blotting 4 h postinjection. The CQ injection resulted in a statistically significant increase in the levels of LC3-II, as well as LC3-I and SQSTM1 (Fig. 6), confirming that CQ reaches the retina and exerts its inhibitory effect as expected. However, CQ-induced LC3-II increase (reflecting the autophagy flux) in Rho$^{P23H/WT}$/Tsc2$^{Rod\ KO}$ and Tsc2$^{Rod\ KO}$ retinas was indistinguishable from changes in Rho$^{P23H/WT}$ and WT littermate mice. This indicates that rod-Tsc2 knockout does not lead to measurable changes in autophagy, at least as assessed by this method. This finding is not particularly surprising because previous observations showed that genetic disruption of Tsc1/Tsc2 may not affect autophagy in neurons due to the AMPK-mediated compensatory feedback (32).

Next, we used puromycin labeling to assess potential changes in protein translation. This approach is based on puromycin's ability to incorporate into growing polypeptide chains, which could be detected using anti-puromycin antibody. Changes in the intensity of puromycin staining in Western blots of cellular extracts reflect the efficiency of protein translation both in vitro and in vivo and were previously used in studies of the retina (33–36).

Mice were injected intraperitoneally with puromycin as described (36). Thirty minutes later, their retinas were harvested, and the expression of puromycin-modified proteins was analyzed by Western blotting. To specifically identify puromycin-labeled polypeptides, we ran samples from puromycin-injected

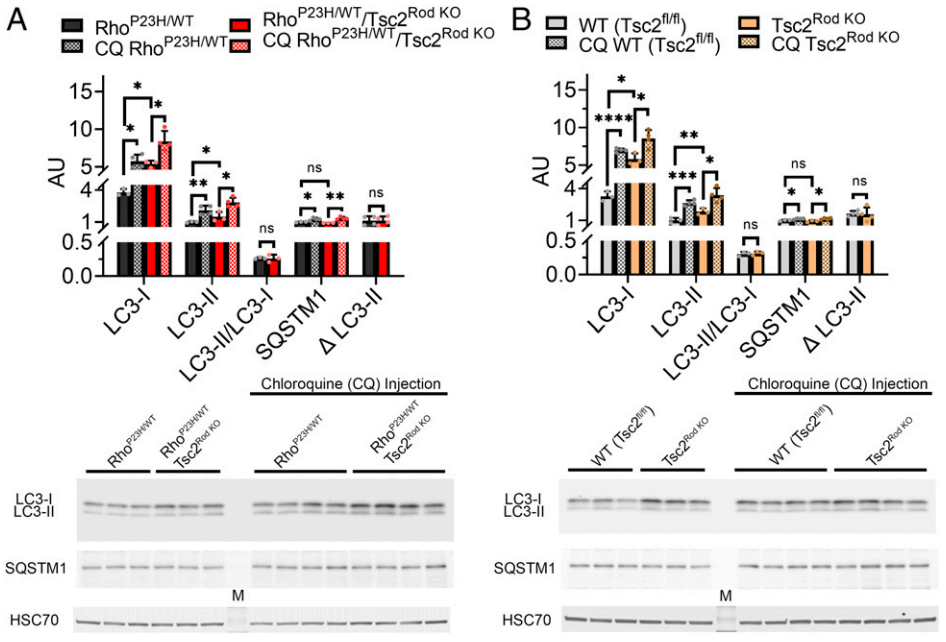

Fig. 6. Rod-specific Tsc2 knockout does not change autophagy flux. (*A* and *B*) Western blots (*Bottom*) and quantification plots (*Top*) of comparative changes in autophagy markers caused by CQ injections 4 h before the retina collection. Data are normalized on the average density of LC3-II or SQSTM1 levels of the untreated group for Rho$^{P23H/WT}$ or WT (Tsc2$^{fl/fl}$) littermate mice. All animals are 1 mo old. Representative results from three independent experiments for each mouse line are shown. The infrared (HSC70) and ECL (LC3 and SQSTM1) Western blotting systems were used for protein detection. The bands (indicated with M) between CQ-treated and -untreated groups on HSC70 blots correspond to the prestained protein markers detected with Odyssey Image System. *$P < 0.05$, **$P < 0.01$, ***$P < 0.001$, ****$P < 0.0001$, and ns for $P > 0.05$.

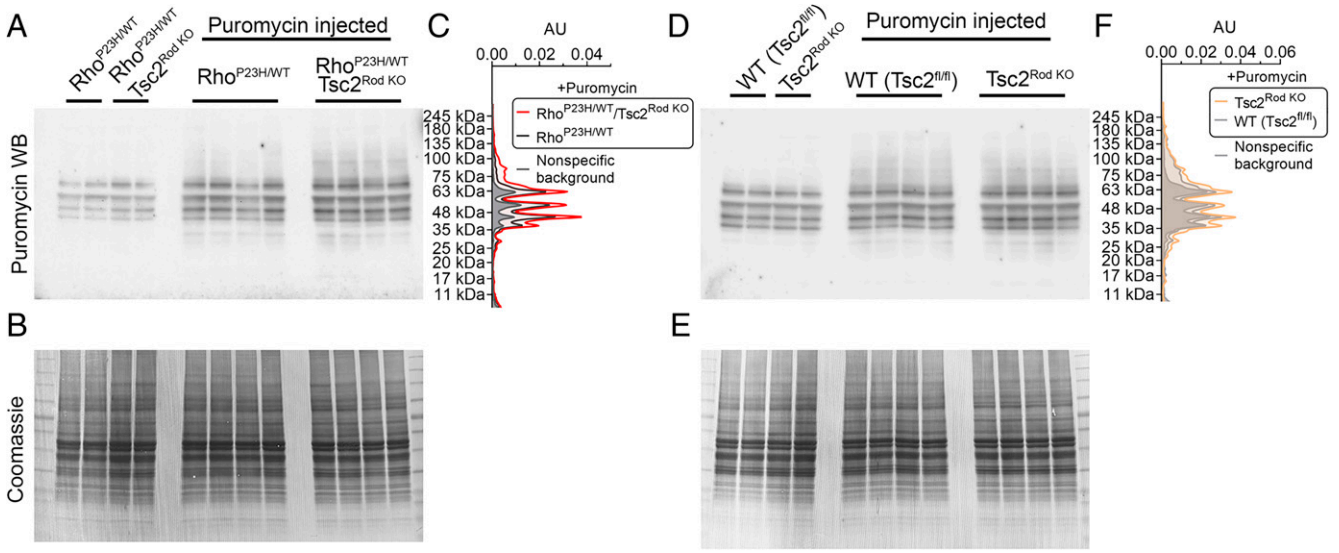

Fig. 7. Rod-specific Tsc2 knockout stimulates protein translation. (*A* and *D*) Puromycin staining of Western blot membranes of retinal lysates prepared from mice injected with puromycin 30 min prior to the analysis. Retinal lysates from uninjected mice were used to control for nonspecific properties of the anti-puromycin antibody. (*B* and *E*) Coomassie staining of the membrane shown in *A* and *D*. (*C* and *F*) Average density profile of puromycin staining for blots shown in *A* and *D* were normalized on the density values of Coomassie-stained membranes. Representative results from three (for $Rho^{P23H/WT}/Tsc2^{Rod\ KO}$ mouse line) and four (for $Tsc2^{Rod\ KO}$ mouse line) independent experiments are shown. AU: arbitrary unit, WB: western blot. All animals are 1 mo old.

and uninjected mice on the same gel. Western blots of the retinas from uninjected mice showed four prominent nonspecific bands in the 35 to 75 kDa region (Fig. 7*A*). These nonspecific bands became notably darker in retinal extracts obtained from puromycin-injected mice; the reasons for these changes are not clear. However, we also noted additional staining above and below the 35 to 75 kDa region, which was not present in uninjected mice and most likely corresponded to puromycin-modified proteins. The overall density profile was notably darker in the retinas of $Rho^{P23H/WT}/Tsc2^{Rod\ KO}$ mice in comparison to $Rho^{P23H/WT}$ littermates, including the blot areas above the 75 and below the 35 kDa markers (Fig. 7*C*). Similarly, a more intense puromycin staining was found in the retinas of $Tsc2^{Rod\ KO}$ mice in comparison to WT littermates (Fig. 7). These data indicate that rod-Tsc2 knockout stimulates protein translation in both $Rho^{P23H/WT}/Tsc2^{Rod\ KO}$ and $Tsc2^{Rod\ KO}$. This is consistent with higher levels of phosphorylated 4E-BP1 and S6K1 proteins described above (Fig. 1), which serve as markers of elevated protein translation.

Taken together, our analysis of proteostatic branches demonstrates that rod-specific Tsc2 knockout counteracts UPS insufficiency in $Rho^{P23H/WT}$ mice, and it could not be explained by increased autophagic activity or decreased levels of protein translation.

Increased Proteasomal Activity in Rod-Specific Tsc2 Knockout Mice Is Phosphorylation Dependent. Previous studies in mouse embryonic fibroblasts and mouse brains showed that genetic deletion of Tsc1 and Tsc2 stimulates proteasomal biogenesis (8, 15). Therefore, in the final set of the experiments, we investigated whether better clearance of the UPS reporter in rods of $Rho^{P23H/WT}/Tsc2^{Rod\ KO}$ could be attributed to higher proteasomal content and activity.

Since the proteasome consists of multiple proteins, we limited the analysis to representative subunits of its key components (the core 20S particle and its 19S, 11S, and PA200 regulators) (12, 37). The retinas of $Tsc2^{Rod\ KO}$ mice (Fig. 8 *A* and *B*) contained ∼25 to 35% higher levels of the representative subunits of the core 20S particle (α1-α7 and β5) and the 19S regulator (PSMD1, PSMD11). Although these changes were small, they are likely low-end estimates since Tsc2 was removed not in the entire retina but only in rods. The increased levels of PSMD11 and β5 were particularly interesting since overexpression of each of these subunits increased the resistance to proteotoxic stressors and correlated with higher proteasomal activity in cell culture studies, although the underlying mechanisms in each case are not currently understood (38, 39).

A different proteasomal expression response was found in $Rho^{P23H/WT}/Tsc2^{Rod\ KO}$ mice (Fig. 8 *A* and *B*). Rod-Tsc2 knockout did not change the levels of essential α1-α7 and PSMD1 subunits, but the expression of PSMD11 and β5 proteasomal subunits was consistently higher, which reached statistical significance in experiments repeated multiple times. Changes in the levels of ubiquitin-independent regulators (11S α and PA200) were not noted. Transcriptional analysis using qRT-PCR showed elevated transcripts for 20S and 19S components in both $Rho^{P23H/WT}/Tsc2^{Rod\ KO}$ and $Tsc2^{Rod\ KO}$ mouse lines; however, effects in $Rho^{P23H/WT}/Tsc2^{Rod\ KO}$ were smaller (Fig. 8*C*). A master regulator of proteasomal transcription, Nfe2l1 (nuclear factor erythroid 2-related factor 1), had elevated transcripts in $Tsc2^{Rod\ KO}$ but not $Rho^{P23H/WT}/Tsc2^{Rod\ KO}$ retinas (8, 40).

Next, we measured the major (chymotrypsin-like) proteolytic activity of proteasomes using a fluorogenic peptide substrate. These measurements showed an ∼22% elevated activity of proteasomes in retinal extracts prepared from both $Rho^{P23H/WT}/Tsc2^{Rod\ KO}$ and $Tsc2^{Rod\ KO}$ mouse lines (Fig. 8*D*). Similar to proteasomal expression, these changes are most likely low-end estimates since Tsc2 was removed only in rod photoreceptors. Furthermore, small changes in the enzymatic activity of the proteasome might have significant effects on the degradation of ubiquitinated proteins in a cellular context.

A nearly identical increase in proteasomal activity in $Tsc2^{Rod\ KO}$ and $Rho^{P23H/WT}/Tsc2^{Rod\ KO}$ mouse lines was surprising, considering different changes in the expression of proteasomal subunits (Fig. 8 *A* and *B*). This prompted us to seek alternative mechanisms driving higher proteolytic activity that is not connected to proteasomal biogenesis. Recent studies revealed that proteasomal activity

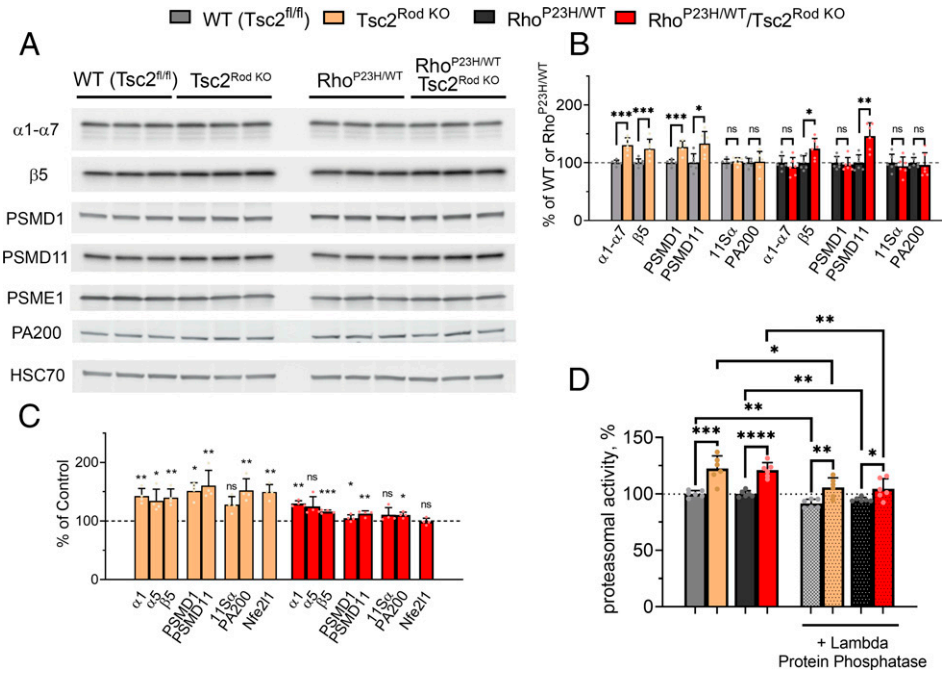

Fig. 8. Proteasomal expression and activity in the retinas of the rod-specific Tsc2 knockout mice. (*A*) Representative Western blots and (*B*) quantification graphs of proteasomal components detected in the retinal extracts prepared from mice of the indicated genotypes. (*C*) Transcriptional analysis of representative proteasomal subunits performed using qRT-PCR. (*D*) Chymotrypsin-like proteasomal activity measured in the retinal extracts treated or untreated with lambda protein phosphatase. Quantification plots are normalized on the average values for WT ($Tsc2^{fl/fl}$) or $Rho^{P23H/WT}$ littermate mice. All animals are 1 mo old. $*P < 0.05$, $**P < 0.01$, $***P < 0.001$, $****P < 0.0001$, and ns for $P > 0.05$.

could be modulated by various phosphorylation mechanisms (reviewed in 41). mTORC1 is a potent kinase complex with a large number of targets. Although mTORC1 has not been linked to the phosphorylation of proteasomal subunits, we hypothesized that higher proteasomal activity in rod-Tsc2 knockout retinas could be explained by phosphorylation changes. To test this hypothesis, we measured changes in proteasomal activity in retinal lysates after treatment with lambda protein phosphatase, a potent enzyme with activity toward phosphorylated serine, threonine, and tyrosine residues (Fig. 8*D*). The phosphatase treatment of retinal extracts led to nearly complete loss of differences in proteasomal activity caused by rod-Tsc2 knockout. This shows that increased proteolytic activity in rod-Tsc2 knockout lines is mostly phosphorylation-sensitive. Yet even after phosphatase treatment, the proteasomal activity in $Tsc2^{Rod\,KO}$ and $Rho^{P23H/WT}/Tsc2^{Rod\,KO}$ remained slightly higher in comparison to WT and $Rho^{P23H/WT}$ mice, indicating that a portion of mTORC1-controlled activity might have a different origin.

Discussion

mTORC1 is one of the most complex cellular systems. The most studied aspects of the mTORC1 pathway are its ability to modulate protein translation, autophagy, and cellular metabolism (27–29, 42, 43). Here we report that in a mouse model of human blindness caused by misfolded rhodopsin, the genetic activation of mTORC1 through deletion of its negative regulator Tsc2 (1) counteracts ubiquitin-proteasome insufficiency, (2) stimulates proteasomal activity through phosphorylation, (3) delays photoreceptor loss, and improves visual function.

A burgeoning area in the field of cellular proteostasis is the complex mutual dependence and regulation of the mTORC1 pathway and UPS, as both activation and inhibition of mTORC1 have previously been reported to improve the degradation of ubiquitinated proteins (8–15). Our study suggests that genetic activation of mTORC1 stimulates the degradation of ubiquitinated proteins in degenerating photoreceptor neurons. Current methods do not allow us to fully assess in vivo which of the signaling pathways controlled by mTORC1 reduced the accumulation of the proteasomal reporter in $Rho^{P23H/WT}/Tsc2^{Rod\,KO}$ mouse rods. This could have been achieved through a direct increase in proteasomal activity, a more complex modulation of the UPS (e.g., through changes in the efficiency of protein ubiquitination/deubiquitination), or indirectly through metabolic changes (e.g., changes in glucose, nucleotide, lipid synthesis, and energy metabolism). Regardless, our data show that decreased levels of UPS reporter in $Rho^{P23H/WT}/Tsc2^{Rod\,KO}$ rods could not be explained by higher levels of autophagy or slower rates of protein translation. Our observations encourage further mechanistic studies of mTORC1/UPS regulation and highlight the potential to harness the complexity of their regulation for clinical applications. A better understanding of UPS-mTORC1 interconnection, complex experimental methods, and new animal models would be required to separate the numerous aspects of mTORC1 signaling in their influence on rod protection and the regulation of the UPS.

An actively debated topic is whether activation of mTORC1 could modulate the abundance and activity of proteasomes (8, 12, 13). In this study, we observed a small but coordinated increase in the transcript and protein levels of essential 20S and 19S proteasomal subunits in the retinas of rod-Tsc2 knockout mice. In degenerating retinas of $Rho^{P23H/WT}/Tsc2^{Rod\,KO}$ mice, we found slightly higher protein expression of individual proteasomal subunits (PSMD11 and β5), while the levels of other essential structural subunits remained apparently unchanged. This was accompanied by a smaller transcriptional response than in $Tsc2^{Rod\,KO}$ mice, which may potentially account for the observed differences in proteasomal expression. Nevertheless, higher levels of proteasomal transcripts in both rod-Tsc2

knockout mouse lines are consistent with the proposed role of the mTORC1 in transcriptional regulation of proteasomal subunits (8). The mechanisms regulating proteasomal expression by mTORC1 are currently unknown but might include Srebf1 (sterol regulatory element-binding transcription factor 1) and Nfe2l1 transcriptional factors (8, 15). Our observations in photoreceptor cells call for further studies of mTORC1-mediated transcriptional regulation of proteasomes and warn about potential differences in response in degenerating cells.

We found that despite different changes in the expression of individual proteasomal subunits, rod-Tsc2 deletion led to a similar increase in proteasomal activity in $Tsc2^{Rod\,KO}$ and $Rho^{P23H/WT}/Tsc2^{Rod\,KO}$ mouse lines. This difference inspired us to seek an alternative explanation for higher proteasomal activity. A growing number of studies shows that proteasomal activity can be modulated by phosphorylation. Proteomic analysis suggests that more than 400 phosphorylation sites are present in the proteasome. Phosphorylation of proteasomal subunits by several serine-threonine kinases, including dual-specific tyrosine-regulated kinase 2, protein kinases A and G, c-Abl tyrosine kinase, and p38 mitogen-activated protein kinases, were reported to activate and inhibit proteasomal activity (reviewed in 41). mTORC1 is a kinase complex with a broad network of phosphorylation targets, which, according to global proteomics studies, may include at least 500 different proteins (44). However, mTORC1 has not previously been linked to the regulation of proteasomal activity through phosphorylation. We now found that proteasomal activity measured in retinal extracts of rod-specific Tsc2 mice is phosphorylation-dependent. This observation opens exciting avenues to study the role of mTORC1 in the regulation of proteasomal activity in the cellular context not only through proteasomal biogenesis but also through phosphorylation. Future studies should establish whether this was achieved directly through phosphorylation of proteasomes or indirectly through phosphorylation of proteasome-interacting proteins. These studies should also specify whether mTORC1 could modify proteasomal activity directly or indirectly, e.g., through the activation of other kinases.

Finally, we should point out that the therapeutic potential of mTORC1 activation was previously investigated in genetically diverse mouse models of retinal degeneration. Activation of the mTORC1 pathway was reported to delay nonautonomous cone death caused by rod photoreceptor-specific mutations, increased resistance of the retina to RPE injury caused by the strong oxidizing agent sodium iodate, slowed down the early stages of degeneration in *PDE6b* (phosphodiesterase 6β) mutant mice for 1 wk, and preserved the number of photoreceptors in young rd16 mice (35, 45–49). These studies attributed retinal preservation to improved glucose metabolism, restoration of the translation rate, and changes in autophagy. Our study suggests that mTORC1 activation could also modulate proteasomal activity and processing of ubiquitinated proteins. We observed that Tsc2 knockout delayed photoreceptor loss in $Rho^{P23H/WT}$ but failed to halt it. Therefore, the beneficial effects caused by Tsc2 knockout did not eliminate stress caused by misfolded rhodopsin. Further mechanistic studies and consideration of the complexity of mTORC1 signaling are required in exploring the therapeutic potential of mTORC1 activation to treat or delay retinal degeneration in a gene-independent manner.

Materials and Methods

Animals and Animal Procedures. The $Tsc2^{fl/fl}/iCre75^{+/-}$ (abbreviated as $Tsc2^{Rod\,KO}$ in the text) mouse line was derived by crossing $Tsc2^{fl/fl}$ (Jackson Labs, stock # 027458) and iCre75 (Jackson Labs, stock # 015850) mouse lines. The $Rho^{P23H/P23H}$ mice were purchased from Jackson Labs (stock # 017628). Transgenic mice expressing the Ub^{G76V}-GFP proteasomal reporter were obtained from the colony of Vadim Arshavsky (Duke University, Durham, NC). $Rho^{P23H/WT}/Tsc2^{Rod\,KO}$ and $Rho^{P23H/WT}$ littermate mice were obtained by crossing $Rho^{P23H/P23H}/Tsc2^{fl/fl}$ and $Tsc2^{Rod\,KO}$ mice.

Animals were reared under a normal day/night cycle and handled according to the protocols approved by the Institutional Animal Care and Use Committee of the University of Florida. Littermates of both sexes were used and processed as a group. Mouse genotypes were determined using real-time PCR with specific probes designed for each gene (Transnetyx). All lines were tested negative for *rd1* and *rd8* mutations.

Noninvasive experiments were performed under ketamine/xylazine anesthesia (100/10 mg/kg). The pupils of mouse eyes were dilated with a drop of TropiPhen ophthalmic solution (PINE Pharmaceuticals). During procedures, mouse eyes were kept lubricated with GenTeal or Systane Eye Drops. After measurements, mice were injected with 5 mg/kg of Antisedan (ZOETIS) to accelerate recovery from anesthesia.

Funduscopic images were acquired using the Micron IV system (Phoenix Technology Group). SD-OCT (spectral domain-optical coherence tomography) images were acquired with the Envisu SD-OCT Ophthalmic imaging system (Leica Microsystems). OCT images were collected in 1.2 mm × 1.2 mm rectangular area around optic nerve with scanning parameters 850/85/1/1 (A/B-scan/B-scan/frame/volume). The ONL thickness was determined manually from OCT images as a distance between the outer plexiform layer and the OLM) using the Straight Line Tool and Bioptogen plugin in ImageJ software. The scale was set based on the pixel to millimeter ratio, and measurements were made along the horizontal axes of the collected scans.

ERG (electroretinography) measurements were performed on dark-adapted mice using the Espion E2 system with a ColorDome ganzfeld stimulator (Diagnosys LLC) following a previously described protocol (5). Responses from both eyes were recorded simultaneously using N1530NNCD200 electrodes (LKC Technologies). The stainless steel needle placed in the mouth was used as a reference. A needle positioned at the base of the tail was used as a ground electrode. The a- and b-waves were measured manually after plotting individual ERG recordings in GraphPad Prism Software, and the b-wave was measured at the maximum of the response. The summary plots for a- and b-waves were fitted with single and double hyperbolic equations.

An assessment of protein translation assays was performed in whole retinal extracts, as described in the previous retinal studies (36). Briefly, mice were intraperitoneally injected with puromycin (P8833, Sigma) dissolved in PBS (phosphate buffered saline) and injected at the dose of 0.04 μmol/g body weight. Their retinas were collected 30 min after injections, dissected in Hanks Balanced Salt Solution (HBSS), flash-frozen, and stored at −80 °C until used. Puromycin-modified proteins were detected using primary mouse anti-puromycin and secondary anti-mouse IgG2a antibodies listed in the antibodies section and selected based on previous studies (34, 36). The ECL (enhanced chemiluminescence) signal for puromycin blots required a prolonged ∼10 min exposure. Experiments were performed in 1-mo-old littermate mice between 12 and 1 PM.

The autophagy flux was evaluated following previously reported retinal protocols (50, 51). Briefly, half of the mice of each genotype was injected with CQ (02193919, MP Biomedicals) dissolved in PBS at the dose of 50 mg/kg body weight 4 h before the tissue collection. Their retinas were collected at 1 PM, flash-frozen, and stored at −80 °C until used. The autophagy flux (Δ LC3-II) was assessed based on the differences in the levels of the LC3-II marker after CQ treatment, as described in the references (30, 31).

Antibodies. Mouse anti-20S α1, 2, 3, 5, 6, 7 (BML-PW8195), rabbit anti-PSME1 (BML-PW8185), and anti-Hsc70 (ADI-SPA-819) antibodies were from Enzo Life Sciences. Rabbit anti-PSMB5 (ab3330) and anti-PSMD1 (ab140682) antibodies were from Abcam. Rabbit anti-PSMD11 (NBP1-46192) antibody was from Novus Biologicals. Rabbit antibodies against Tsc2 (4308T), phospho-p70 S6 kinase (9234T), p70 S6 kinase (2708), phospho-4E-BP1 (2855), 4E-BP1 (9644), and LC3A/B (4108) were from Cell Signaling Technology. Rabbit anti-GFP (A11122) and mouse anti-beta actin (MA5-15739-D800) antibodies were from Invitrogen. The mouse anti-puromycin (MABE343) antibody was from EMD Millipore. Secondary anti-mouse and anti-rabbit antibodies conjugated with Alexa

Fluor 680 (A-21057) and 800 (SA5-10044) were from Invitrogen. The secondary anti-rabbit (711-035-152) and anti-mouse (711-035-150 and 115-035-206) antibodies conjugated with horseradish peroxidase were from Jackson Immuno Research Laboratories Inc.

Histology and Microscopy. For the morphometric studies, mice were transcardially perfused with 3 mL of 2% paraformaldehyde and 2.5% glutaraldehyde fixative solution in PBS buffer at a flow rate of 1 to 2 mL/min. The orientation of the eye was marked with low-temperature cautery (AA90, Bovie). Next, the eyes were enucleated, fixed overnight at 4 °C in the same fixative, rinsed, and embedded in paraffin. The 4-μm-thick paraffin sections cut through the superior-inferior line through the optic nerve were stained with hematoxylin and eosin stain (H&E) and imaged on a wide-field DMi8 Leica fluorescence microscope. The nuclear count was performed in sections cut through the optic nerve in 100-μm segments of the ONL at different distances from the ONH as described (5).

An accumulation of the Ub^{G76V}-GFP reporter was assessed in 20-μm-thick frozen retinal sections prepared from the eyes fixed in 4% paraformaldehyde PBS solution (52). Outer segments of the rods were stained with WGA (wheat germ agglutinin, Alexa Fluor 555 conjugate, W32464, Thermo Fisher). Samples were processed in parallel and imaged on a Leica TCS SP8 confocal microscope using the same settings.

Proteasome Activity Assays with Fluorogenic Peptides. Two retinas from one mouse were homogenized on ice with Dounce homogenizer (2 mL) in 700 μl of the assay buffer (50 mM Tris·HCl [pH 7.6], 40 mM KCl, 1 mM $MnCl_2$, 5 mM $MgCl_2$, 1 mM DTT (dithiothreitol), 5 mM ATP (adenosine triphosphate), 10% glycerol) followed by centrifugation for 20 min at 18,000 × g at 4 °C. The proteasomal activity was assessed in 200 μL of diluted supernatants containing 10 μg of protein with 100 μM Suc-LLVY-AMC (UbpBio) chymotrypsin-like fluorogenic substrate. The measurements were performed with or without λ protein phosphatase (NEB, P0753S, 10 unit/μg of protein in retinal lysate). Protein phosphatase was diluted in the PMP (Protein MetalloPhosphatase) buffer provided with the phosphatase kit; the PMP buffer was used with untreated control samples. The time course of the AMC fluorescence increase was monitored at 37 °C with CLARIOstar (BMG Labtech). The proteasomal activity was assessed from the slope measurements of linearly fitted fluorescence curves with MARS Data Analysis Software. Measurements were normalized on the total protein amount and expressed as a percentage of the average values for untreated $Rho^{P23H/WT}$ or WT ($Tsc2^{fl/fl}$) littermate mice. To distinguish proteasomal activities from other potential proteolytic activities in retinal extracts, measurements were performed with and without 5 μM proteasomal inhibitor epoxomicin (F1400, UBPBio).

Transcriptional Analysis. The transcript levels of proteasomes and other genes were measured and quantified using the qRT-PCR delta-delta Ct method. Total RNA was extracted using the RNAeasy Mini Kit (QIAGEN), and the RNA concentration was determined using NanoDrop OneC (Thermo Scientific). cDNA (complementary DNA) was synthesized from 1 μg of total RNA using the Verso cDNA Synthesis Kit (Thermo, AB1453A) with oligo-(dT) primers according to the manufacturer's instructions. Signals of transcripts were obtained on a sequence-detection system (CFX Connect; Bio-Rad) using SYBR-Green (Apex qPCR GREEN Master Mix, 42-116PG) and normalized to signals for an endogenous reference Hsc70 (heat shock cognate 71 kDa protein). Changes in expression levels of proteasomal genes were calculated as a percentage of the average values for littermate mice. Primer sets (*SI Appendix*, Table S1) were selected using the Primer3 program and validated for efficiency with serial dilutions of cDNA.

Western Blotting. Retinas from mice of indicated ages were collected between 12 and 2 PM, carefully dissected in HBSS, snap-frozen in liquid nitrogen, and stored at −80 °C until use. Retinas were solubilized by sonicating in 200 μL of RIPA lysis buffer (20-188, EMD Millipore) supplemented with a protease inhibitor mixture (Roche) and a protease phosphatase inhibitor (Thermo Fisher Scientific). The total protein concentration was measured using the Pierce 660 nm Protein Assay Reagent (Thermo Fisher Scientific). Samples were brought to the same concentration in Laemmli buffer, heated at 95 °C for 5 min, and immediately used for experiments. Samples containing 20 to 40 μg of total protein were resolved on the precast 4 to 20% Tris-glycine gel (5671094, Bio-Rad Laboratories), transferred to a 0.45-μm PVDF (polyvinylidene fluoride) membrane (IPFL00010, EMD Millipore) by wet Western blot transfer, blocked, and used for protein detection. The membranes were blocked in either Tris-based Odyssey Blocking Buffer (LI-COR Biosciences) or TBST (20 mM Tris·HCl, pH 8.0, 0.1% Tween-20) solution containing 5% of ECL Prime Blocking Reagent (RPN418, GE Healthcare Life Sciences). After blocking, membranes were incubated overnight with the primary antibody in a cold room, washed, incubated with secondary antibodies for 1 h at room temperature, washed again, and further used for imaging. Protein bands were visualized with the Odyssey Infrared Imaging System (LI-COR Biosciences) or ChemiDoc Imager system (Bio-Rad Laboratories). Enhanced chemiluminescent reactions were developed using the ProSignal Pico ECL reagent (20-300, Genesee Scientific). Western blots were quantified using ImageJ.

Statistical Analysis. Statistical analysis was performed in GraphPad Prism 8 software or Excel for Microsoft 365. Results are presented as the mean ± SD unless noted otherwise. Differences are considered significant for P value <0.05, as determined by a two-tailed Student's test. P values on the figures are indicated as follows: $*P<0.05$, $**P<0.01$, $***P<0.001$, $****P<0.0001$, and ns for $P>0.05$.

Data Availability. All data generated or analyzed during this study are included in the published article and its supplementary information files.

ACKNOWLEDGMENTS. This work was supported by NIH Grants EY030043 (E.S.L.), EY031720 (J.D.A.), and S10D028476; University of Florida startup funds (E.S.L.); and an unrestricted grant from the Research to Prevent Blindness Foundation to the Department of Ophthalmology of the University of Florida. We thank Drs. Vadim Arshavsky and Clay Smith for discussion of this work.

Author affiliations: [a]Department of Ophthalmology, University of Florida, Gainesville, FL 32610; [b]Department of Ophthalmology and Visual Sciences, University of Massachusetts Medical School, Worcester, MA 01655; and [c]Department of Pharmacology and Therapeutics, University of Florida, Gainesville, FL 32610

1. L. Ziccardi *et al.*, Gene therapy in retinal dystrophies. *Int. J. Mol. Sci.* **20**, E5722 (2019).
2. M. Menghini, J. Cehajic-Kapetanovic, R. E. MacLaren, Monitoring progression of retinitis pigmentosa: Current recommendations and recent advances. *Expert Opin. Orphan Drugs* **8**, 67–78 (2020).
3. F. S. Sorrentino, C. E. Gallenga, C. Bonifazzi, P. Perri, A challenge to the striking genotypic heterogeneity of retinitis pigmentosa: A better understanding of the pathophysiology using the newest genetic strategies. *Eye (Lond.)* **30**, 1542–1548 (2016).
4. E. S. Lobanova, S. Finkelstein, N. P. Skiba, V. Y. Arshavsky, Proteasome overload is a common stress factor in multiple forms of inherited retinal degeneration. *Proc. Natl. Acad. Sci. U.S.A.* **110**, 9986–9991 (2013).
5. E. S. Lobanova *et al.*, Increased proteasomal activity supports photoreceptor survival in inherited retinal degeneration. *Nat. Commun.* **9**, 1–11 (2018).
6. Y. P. Liu *et al.*, Ciliopathy proteins regulate paracrine signaling by modulating proteasomal degradation of mediators. *J. Clin. Invest.* **124**, 2059–2070 (2014).
7. H. Xu, N. Enemchukwu, X. Zhong, O. Zhang, Y. Fu, Deletion of M-Opsin prevents M cone degeneration in a mouse model of Leber Congenital Amaurosis. *Am. J. Pathol.* **190**, 1059–1067 (2020).
8. Y. Zhang, B. D. Manning, mTORC1 signaling activates NRF1 to increase cellular proteasome levels. *Cell Cycle* **14**, 2011–2017 (2015).
9. J. Zhao, A. L. Goldberg, Coordinate regulation of autophagy and the ubiquitin proteasome system by MTOR. *Autophagy* **12**, 1967–1970 (2016).
10. J. Zhao, G. A. Garcia, A. L. Goldberg, Control of proteasomal proteolysis by mTOR. *Nature* **529**, E1–E2 (2016).
11. A. Rousseau, A. Bertolotti, An evolutionarily conserved pathway controls proteasome homeostasis. *Nature* **536**, 184–189 (2016).
12. A. Rousseau, A. Bertolotti, Regulation of proteasome assembly and activity in health and disease. *Nat. Rev. Mol. Cell Biol.* **19**, 697–712 (2018).
13. O. A. J. Adegoke, B. E. Beatty, S. R. Kimball, S. S. Wing, Interactions of the super complexes: When mTORC1 meets the proteasome. *Int. J. Biochem. Cell Biol.* **117**, 105638 (2019).
14. J. Zhao, B. Zhai, S. P. Gygi, A. L. Goldberg, mTOR inhibition activates overall protein degradation by the ubiquitin proteasome system as well as by autophagy. *Proc. Natl. Acad. Sci. U.S.A.* **112**, 15790–15797 (2015).
15. Y. Zhang *et al.*, Coordinated regulation of protein synthesis and degradation by mTORC1. *Nature* **513**, 440–443 (2014).
16. J. H. Choi *et al.*, mTORC1 accelerates retinal development via the immunoproteasome. *Nat. Commun.* **9**, 1–16 (2018).
17. O. Hernandez, S. Way, J. McKenna III, M. J. Gambello, Generation of a conditional disruption of the Tsc2 gene. *Genesis* **45**, 101–106 (2007).
18. S. Li *et al.*, Rhodopsin-iCre transgenic mouse line for Cre-mediated rod-specific gene targeting. *Genesis* **41**, 73–80 (2005).
19. W. C. Chiang *et al.*, Robust endoplasmic reticulum-associated degradation of Rhodopsin precedes retinal degeneration. *Mol. Neurobiol.* **52**, 679–695 (2015).

20. S. Sakami *et al.*, Probing mechanisms of photoreceptor degeneration in a new mouse model of the common form of autosomal dominant retinitis pigmentosa due to P23H opsin mutations. *J. Biol. Chem.* **286**, 10551–10567 (2011).
21. S. Y. Cheng *et al.*, HK2 mediated glycolytic metabolism in mouse photoreceptors is not required to cause late stage age-related macular degeneration-like pathologies. *Biomolecules* **11**, 871 (2021).
22. S. Y. Cheng *et al.*, Altered photoreceptor metabolism in mouse causes late stage age-related macular degeneration-like pathologies. *Proc. Natl. Acad. Sci. U.S.A.* **117**, 13094–13104 (2020).
23. E. S. Lobanova *et al.*, Transducin gamma-subunit sets expression levels of alpha- and beta-subunits and is crucial for rod viability. *J. Neurosci.* **28**, 3510–3520 (2008).
24. K. Lindsten, V. Menéndez-Benito, M. G. Masucci, N. P. Dantuma, A transgenic mouse model of the ubiquitin/proteasome system. *Nat. Biotechnol.* **21**, 897–902 (2003).
25. N. P. Dantuma, L. C. Bott, The ubiquitin-proteasome system in neurodegenerative diseases: Precipitating factor, yet part of the solution. *Front. Mol. Neurosci.* **7**, 70 (2014).
26. F. A. Salomons, L. G. Verhoef, N. P. Dantuma, Fluorescent reporters for the ubiquitin-proteasome system. *Essays Biochem.* **41**, 113–128 (2005).
27. I. Ben-Sahra, B. D. Manning, mTORC1 signaling and the metabolic control of cell growth. *Curr. Opin. Cell Biol.* **45**, 72–82 (2017).
28. C. C. Thoreen, The molecular basis of mTORC1-regulated translation. *Biochem. Soc. Trans.* **45**, 213–221 (2017).
29. V. Giguère, Canonical signaling and nuclear activity of mTOR-a teamwork effort to regulate metabolism and cell growth. *FEBS J.* **285**, 1572–1588 (2018).
30. D. J. Klionsky *et al.*, Guidelines for the use and interpretation of assays for monitoring autophagy. *Autophagy* **17**, 1-382 (2021).
31. N. Mizushima, T. Yoshimori, How to interpret LC3 immunoblotting. *Autophagy* **3**, 542–545 (2007).
32. A. Di Nardo *et al.*, Neuronal Tsc1/2 complex controls autophagy through AMPK-dependent regulation of ULK1. *Hum. Mol. Genet.* **23**, 3865–3874 (2014).
33. V. Ravi *et al.*, Systematic evaluation of the adaptability of the non-radioactive SUnSET assay to measure cardiac protein synthesis. *Sci. Rep.* **8**, 4587 (2018).
34. C. A. Goodman, T. A. Hornberger, Measuring protein synthesis with SUnSET: A valid alternative to traditional techniques? *Exerc. Sport Sci. Rev.* **41**, 107–115 (2013).
35. I. V. Saltykova *et al.*, Tribbles homolog 3-mediated targeting the AKT/mTOR axis in mice with retinal degeneration. *Cell Death Dis.* **12**, 664 (2021).
36. C. R. Starr, P. M. Pitale, M. Gorbatyuk, Translational attenuation and retinal degeneration in mice with an active integrated stress response. *Cell Death Dis.* **9**, 484 (2018).
37. G. A. Collins, A. L. Goldberg, The logic of the 26S proteasome. *Cell* **169**, 792–806 (2017).
38. D. Vilchez *et al.*, Increased proteasome activity in human embryonic stem cells is regulated by PSMD11. *Nature* **489**, 304–308 (2012).
39. N. Chondrogianni *et al.*, Overexpression of proteasome beta5 assembled subunit increases the amount of proteasome and confers ameliorated response to oxidative stress and higher survival rates. *J. Biol. Chem.* **280**, 11840–11850 (2005).
40. A. Northrop, H. A. Byers, S. K. Radhakrishnan, Regulation of NRF1, a master transcription factor of proteasome genes: Implications for cancer and neurodegeneration. *Mol. Biol. Cell* **31**, 2158–2163 (2020).
41. X. Guo, X. Huang, M. J. Chen, Reversible phosphorylation of the 26S proteasome. *Protein Cell* **8**, 255–272 (2017).
42. H. Antikainen, M. Driscoll, G. Haspel, R. Dobrowolski, TOR-mediated regulation of metabolism in aging. *Aging Cell* **16**, 1219–1233 (2017).
43. Z. Mao, W. Zhang, Role of mTOR in glucose and lipid metabolism. *Int. J. Mol. Sci.* **19**, E2043 (2018).
44. Y. Zhang, Y. Zhang, Y. Yu, Global phosphoproteomic analysis of insulin/Akt/mTORC1/S6K signaling in rat hepatocytes. *J. Proteome Res.* **16**, 2825–2835 (2017).
45. L. Petit, C. Punzo, mTORC1 sustains vision in retinitis pigmentosa. *Oncotarget* **6**, 16786–16787 (2015).
46. C. Punzo, K. Kornacker, C. L. Cepko, Stimulation of the insulin/mTOR pathway delays cone death in a mouse model of retinitis pigmentosa. *Nat. Neurosci.* **12**, 44–52 (2009).
47. A. Venkatesh *et al.*, Activated mTORC1 promotes long-term cone survival in retinitis pigmentosa mice. *J. Clin. Invest.* **125**, 1446–1458 (2015).
48. M. Zieger, C. Punzo, Improved cell metabolism prolongs photoreceptor survival upon retinal-pigmented epithelium loss in the sodium iodate induced model of geographic atrophy. *Oncotarget* **7**, 9620–9633 (2016).
49. L. Zhang *et al.*, Reprogramming towards anabolism impedes degeneration in a preclinical model of retinitis pigmentosa. *Hum. Mol. Genet.* **25**, 4244–4255 (2016).
50. Y. Qiu, J. Yao, L. Jia, D. A. Thompson, D. N. Zacks, Shifting the balance of autophagy and proteasome activation reduces proteotoxic cell death: A novel therapeutic approach for restoring photoreceptor homeostasis. *Cell Death Dis.* **10**, 547 (2019).
51. J. Yao *et al.*, Inhibiting autophagy reduces retinal degeneration caused by protein misfolding. *Autophagy* **14**, 1226–1238 (2018).
52. E. S. Lobanova *et al.*, Transducin translocation in rods is triggered by saturation of the GTPase-activating complex. *J. Neurosci.* **27**, 1151–1160 (2007).